IEEE Access
Multidisciplinary | Rapid Review | Open Access Journal

Received 2 January 2024, accepted 10 January 2024, date of publication 17 January 2024, date of current version 25 January 2024.

Digital Object Identifier 10.1109/ACCESS.2024.3355135

RESEARCH ARTICLE

Multi-Functional Wideband Metasurface: Perfect Absorber and Linear to Linear and Linear to Circular Polarization Converter

HUU LAM PHAN[1,2], THI QUYNH HOA NGUYEN[3,4], AND JUNG-MU KIM[4]

[1]Laboratory for Computational Mechanics, Institute for Computational Science and Artificial Intelligence, Van Lang University, Ho Chi Minh City 70000, Vietnam
[2]Faculty of Mechanical-Electrical and Computer Engineering, School of Technology, Van Lang University, Ho Chi Minh City 70000, Vietnam
[3]School of Engineering and Technology, Vinh 460000, Vietnam
[4]Department of Electronic Engineering, Jeonbuk National University, Jeonju 54896, Republic of Korea

Corresponding authors: Thi Quynh Hoa Nguyen (ntqhoa@vinhuni.edu.vn) and Jung-Mu Kim (jungmukim@jbnu.ac.kr)

This research is funded by Vietnam National Foundation for Science and Technology Development (NAFOSTED) under grant number 103.02-2021.44.

ABSTRACT In this paper, a switchable multi-functional wideband metasurface device based on vanadium dioxide (VO_2) in the terahertz (THz) region is numerically proposed. By controlling the phase of VO_2, the functions of the proposed structure can be reversibly switched between a perfect absorber and two different polarization conversions. When VO_2 is in the metallic phase, the absorption response can be achieved with an absorption rate above 0.9 in the range of 1.42 - 4.13 THz for wide-angle incidence, contributed by the highly lossy feature of VO_2 metallic. Meanwhile, when VO_2 acts as an insulator phase, the proposed metasurface exhibits linear-to-linear polarization conversion in the range of 1.27 - 3.53 THz and linear-to-circular polarization conversion in the frequency ranges of 1.08 - 1.24 THz and 3.65 - 5.27 THz simultaneously. This work opens new avenues for realizing multi-functional wideband metasurface devices in the terahertz range.

INDEX TERMS Metasurface, multi-function, wideband, absorption, polarization conversion.

I. INTRODUCTION

Terahertz (THz) technology is of intense interest for both academia and industry based on its unique applications in non-destructive imaging, communications, spectroscopic detection, and sensing [1]. However, the electromagnetic (EM) response of traditional materials in the THz region is very weak owing to its non-ionizing property of terahertz radiation [2].

Recently, metasurfaces, two-dimensional counterparts of metamaterials, have been developed for various applications due to their novel EM features that have not been discovered in natural materials [3], [4]. Additionally, metasurfaces realize a novel approach to manipulate EM waves, leading to various practical applications such as the metalens [5], [6], holograms [7], [8], vortex beam generators [9], [10], waveplates [11], [12], and beam steering [13], [14]. Importantly, the ultrathin nature of metasurfaces, their ease of fabrication, and sub-wavelength resolution for manipulating EM waves make metasurfaces ideal candidates for THz device miniaturization and system integration.

Until now, most of the terahertz metasurfaces have been normally developed for a single functionality, such as absorption [15], [16], [17] and polarization conversion [18], [19], [20], [21], [22]. A novel way to enhance the bandwidth of terahertz polarization conversion is proposed in [19] and [20]. Even though there has been a multi-functional polarization converter based on metasurfaces that displays both linear-to-linear polarization (LP-to-LP) and linear-to-circular polarization (LP-to-CP) conversion [21], [22], they process identical functionalities. Very recently, metasurfaces that can integrate multiple diversified functionalities into one

The associate editor coordinating the review of this manuscript and approving it for publication was Roberta Palmeri.

single device have been proposed using several approaches, such as by integrating the varactor diodes [23], [24] and PIN diodes [25], [26], mechanical shape-changing [27], and stacking ferrite-based elements [28]. Nonetheless, these approaches can only operate in the gigahertz (GHz) region, which significantly limits their applicability in emerging terahertz devices and systems. To overcome this drawback, an alternative approach to realize diversified functionalities is that integrates metasurfaces with active functional materials, including phase-change materials (PCM) [29], [30], [31], [32], [33], [34], [35], [36], [37] and graphene [38], [39], [40]. Compared with graphene material which is difficult in large-scale fabrication, vanadium dioxide (VO_2), a phase change material, suffers a fast response, large modulation depth, and multiple modulation methods [41], as well as a low phase change temperature of $68°C$ [42], therefore it is widely used for THz multi-functional metasurfaces. While PCM-integrated metasurfaces have been successfully designed to obtain active configuration control; however, the operating frequency bands of these metasurfaces are almost not wide for all functionalities and these absorption efficiencies still depend on polarization angle. Song et al. reported VO_2-integrated metasurfaces that exhibited bi-functionalities of broadband LP-to-LP conversion and broadband absorption [43]. Furthermore, Yan et. al. proposed VO_2-assisted broadband absorption and LP-to-CP conversion using a switchable metasurface [44]. However, these polarization conversion and absorption performances are not incident angle stability for both transverse electric (TE) and transverse magnetic (TM) modes [44] or the efficiency of polarization conversion is quite low [43]. More recently, Qiu et. al. proposed a multi-functional design based on VO_2 metamaterial structure that achieved broadband absorption, LP-to-LP conversion, LP-to-CP conversion, and total reflection [32]. However, this design has polarization sensitivity due to the asymmetric structure of the design. Therefore, creating a multi-functional polarization converter with high performance, including wide bandwidth and large incidence angle stability for both LP-to-LP and LP-to-CP conversion, is essential to develop the promising applications.

In this work, we theoretically propose an actively tunable multi-functional wideband metasurfaces that can manipulate switchable functions between absorption and two different polarization conversions in the terahertz frequency. Here, by turning the status of VO_2 materials, the switchable functions can be obtained. When VO_2 is in the metallic state, the broadband absorption response can be obtained with an efficiency above 0.9 in the range of 1.42-4.13 THz. When VO_2 is in the insulator state, the proposed structure exhibits a linear polarization conversion (LPC) response and circular polarization conversion (CPC), simultaneously, where an LPC ratio exceeds 0.9 in the wide frequency range of 1.27-3.53 THz. We expect the metasurface structure demonstrated here to open new possibilities for designing tunable and switchable multi-functional terahertz metamaterial devices.

II. CONCEPT AND DESIGN OF SWITCHABLE MULTI-FUNCTIONAL METASURFACE

The concept and schematic of the multi-functional and broadband metasurface are illustrated in Figs. 1 and 2, respectively. Using the changing the conductivity of VO_2 when it changes phase from metallic to insulator by thermal treatment, the proposed metasurface can switch its functions from absorption (ABS) to polarization conversion (PC) as shown in Fig.1. The proposed multi-functional metasurface structure consists of six layers arranged in order from top to bottom as a VO_2 symmetrical shaped resonator layer (plays as an absorption resonator), silicon dioxide (SiO_2) dielectric layer, gold (Au) diagonal symmetry shaped resonator layer (plays as a polarization conversion resonator), VO_2 layer (plays as switchable function layer), SiO_2 dielectric layer, and gold ground layer (Fig. 2(a)). The absorption resonator layer is designed based on a VO_2 ring-shaped resonator to obtain the broadband absorption feature and polarization insensitivity when the VO_2 stays in the metallic state (Fig. 2(b)). Meanwhile, the previous demonstration usually uses diagonal structure symmetry such as a double split ring shape and elliptic shape to obtain the LPC and CPC, respectively. Here, by modifying the geometric resonator along the diagonal structure from the double split ring to the double split elliptical ring (DSER) (Fig. 2(c)), the proposed metasurface can convert its polarization wave into both LP and CP waves. The geometric parameters of the proposed multi-functional metasurface are shown in Fig. 2.

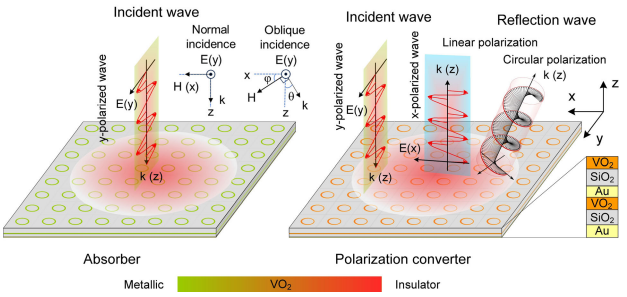

FIGURE 1. Concept of the multi-functional broadband metasurface shows its switchable ability between absorption and polarization conversion modes when VO_2 switches between metallic and dielectric phases.

In this study, the relative permittivity of VO_2 material is given by Drude model [42]:

$$\epsilon(\omega) = \epsilon_\infty - \frac{\epsilon_p^2(\sigma)}{\epsilon^2 + i\gamma\epsilon} \tag{1}$$

with the collision frequency $\gamma = 5.75 \times 10^{13}$ rad/s and epsilon infinity $\epsilon_\infty = 12$ [42]. The plasma frequency can be described by:

$$\epsilon_p^2(\sigma) = \frac{\sigma}{\sigma_o}\epsilon_p^2(\sigma_o) \tag{2}$$

where $\sigma_o = 3 \times 10^5$ S/m and $\epsilon_p^2(\sigma_o) = 1.4 \times 10^{15}$ rad/s. It should be emphasized that VO_2 is a phase transition material. It exhibits the transition state from the insulator

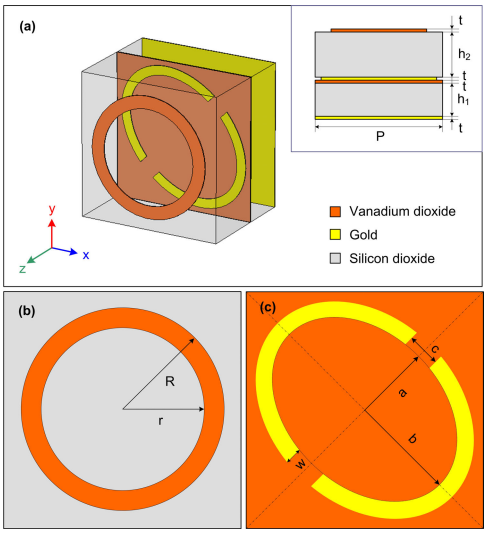

FIGURE 2. Schematic of the proposed multi-functional metasurface: (a) 3D-view of a unit-cell and its side-view, (b) top-view of absorption resonator, and (c) top-view of polarization conversion resonator. The geometric parameters are P=38μm, R=16μm, r=12.6μm, a=15μm, b=20μm, w=2.5μm, c=5μm, h_1=12μm, h_2=17μm, and t=0.2μm.

state to the metal state with increasing temperature higher than the heating point temperature of $68^{\circ}C$ [42], [45]. The conductivity (σ) of VO_2 material is 200 S/m and 2×10^5 S/m, corresponding to a resistivity of 0.5 Ω.cm and 0.5 $\times10^{-3}$ Ω.cm for the insulator phase and metal phase, respectively [42].

It was recently reported that there was good agreement between Computer Simulation Technology (CST) simulations and experimental results of metasurface design such as absorber and polarization converter [22], [25], [38], [46], [47]. Therefore, the CST simulation method through a frequency-domain solver is also used in this work to optimize the design and evaluate the performance of the proposed multi-functional metasurface. We perform the simulation under the unit cell boundary condition in the x- and y- axis and open boundary condition in the z-axis. To obtain the optimize the structure parameters of the proposed structure, it starts with optimizing the dimensions of the top VO_2 resonator, the thickness of the top SiO_2 insulator (h_2), and the period constant of unit cell (P) to obtain the wideband absorption when VO_2 is in its fully metallic state, and then the dimensions of the gold resonator and the thickness of bottom SiO_2 insulator (h_1) to achieve the wideband polarization conversion with the fixed period constant of unit cell when VO_2 is in its insulating state. By this order, the proposed multi-functional metasurface can be systematically tuned for obtaining wideband behavior for both ABS and PC modes. The detail optimization process is shown in Supporting information.

It is noteworthy that the suggested multi-functional metasurface has overall unit cell dimensions of 36 μm$\times$ 36 μm$\times$29.8 μm with six thin layers, which can be manufactured by the existing fabrication methods. The proposed structure in the micro-scale can be patterned using a conventional photo-lithography technique. The thin films of VO_2 and Au can be deposited by a sputtering method, while the SiO_2 thick films can be fabricated by plasma-enhanced chemical vapor deposition (PECVD). The manufacturing process of a similar multi-functional THz metasurface was also proposed in [48]. The previous experimental report indicated that the phase transition of VO_2 could be carried out via thermal treatment using high-vacuum cryostats with temperature control [42]. Furthermore, it has also been demonstrated that the insulator-to-metal transition temperature of VO_2 is less than 1^oC [49]. Therefore, we can assume that the VO_2 is in the insulator-phase at T<68^oC while it is in the metal-phase at the device temperature T>68^oC. For the practical application, a microheater-integrated proposal multi-functional metasurface can be used to control the phase change of VO_2 that can prepared using flexible printed circuit technology [50].

The absorption can be defined from the coefficients of reflection and transmission as $A(\omega) = 1 - R(\omega) - T(\omega)$, where $R(\omega)=|S_{11}|^2$ and $T(\omega) = |S_{21}|^2$. $A(\omega)$, $T(\omega)$, and $R(\omega)$ are the frequency-dependent absorption, transmission, and reflection, respectively. In the design, the transmission can be ruled out because of the EM shielding by the continuous metallic ground.

The LPC efficiency is used to analyze by the polarization conversion ratio (PCR), which is given by Eq.3 [22], [51].

$$PCR = \frac{|r_{xy}|^2}{|r_{xy}|^2 + |r_{yy}|^2} \tag{3}$$

where, r_{xy} and r_{yy} denote the coefficients of cross- and co-polarization reflection for the y-polarized incident wave under normal incidence, which can decrible as Eqs. 4 and 5, respectively [52].

$$|r_{xy}| = \frac{E_{xr}}{E_{yi}} \tag{4}$$

$$|r_{yy}| = \frac{E_{yr}}{E_{yi}} \tag{5}$$

where, E_{yi} and E_{yr} are the electric field of the incident and reflection wave polarized in the y direction, respectively, while E_{xr} is the electric field of the reflection wave polarized in the x direction.

The normalized ellipticity (e) is applied to analyze the degree of the circularly reflected wave, which is defined in Eq. 6 for the y-polarized incident wave [22], [51].

$$e = \frac{2|r_{xy}||r_{yy}|sin\Delta\phi}{|r_{xy}|^2 + |r_{yy}|^2} \tag{6}$$

where, $\Delta\phi = \phi_{yy} - \phi_{xy}$ with ϕ_{yy} and ϕ_{xy} are the phases of co- and cross- polarization reflections, respectively. When the normalized ellipticity (e) is -1, which is equivalent to r_{xy}=r_{yy} and ϕ=$-90^{\circ}+2k\pi$ (k is an integer), the reflection wave is right-handed circularly polarization (RHCP) wave. Meanwhile, when the normalized ellipticity (e) is $+1$, which is equivalent to r_{xy}=r_{yy} and $\Delta\phi$=$90^{\circ}+2k\pi$ (k is an integer),

the reflection wave is left-handed circularly polarization (LHCP) wave.

In addition, the axial ratio (AR) is used to evaluate the CP, described by Eq. 7.

$$AR = 10log\frac{|r_{xy}|}{|r_{yy}|} = 10log\sqrt{\frac{1-cos\Delta\Phi}{1+cos\Delta\Phi}} \quad (7)$$

When the phase difference is $\Delta\phi{=}{\pm}90°{+}2k\pi$ and $|r_{xy}|{=}|r_{yy}|$, the axial ratio is $AR = 0$ dB, the polarized wave is transformed into a circular polarized wave.

III. RESULTS AND DISCUSSION

A. SWITCHABLE FUNCTIONALITIES OF THE PROPOSED METASURFACE

The switchable functionalities from absorption mode to polarization conversion mode of the proposed metasurface can be performed by thermal treatment in order to change the conductivity of the VO_2 material. At room temperature, VO_2 stays in an insulator state with a low conductivity of 200 S/m [42]. Thus, the incoming THz wave may propagate through the top layer of the VO_2 resonator and interact with a metal-insulator-metal (MIM) configuration which corresponds to a gold DSER resonator layer, VO_2 and SiO_2 insulator layer, gold ground layer, resulting in the proposed metasurface can operate at the PC mode. On the contrary, when the temperature is heated higher than the phase-change temperature of $68°C$ [42], VO_2 changes to a fully metallic state and gains its high $2{\times}10^5$ S/m [42]. Therefore, the top VO_2 metallic resonator interacts strongly with the THz wave, while the continuous VO_2 metallic layer can eliminate the transmission. As a result, the first MIM configuration of the top VO_2 metallic resonator, the SiO_2 insulator layer, and the continuous VO_2 metallic layer can work in ABS mode. To evaluate the operating modes of the proposed metasurface, we simulate the conductivity change of VO_2 material from metallic to insulator phases to obtain the absorption and PCR spectra, respectively, as shown in Fig. 3. It is worth noting that the switchable functionalities from ABS mode to PC mode of the proposed metasurface can be obtained by controlling the VO_2 state from metallic to insulator phases. As shown in Fig. 3, when VO_2 is in its metallic state, the proposed metasurface can absorb the normal incident THz wave above 90% in the wide frequency spectrum from 1.42 THz to 4.13 THz, which corresponds to the relative bandwidth (RBW) of 97.7%. Furthermore, when VO_2 is in its metallic state, the simulated PCR spectrum of the proposed metasurface is almost zero in the range of 1.42-4.13 THz (data not shown here). It indicates that the ultra-broadband characteristics of the proposed structure design.

Meanwhile, once VO_2 is in the insulator phase, the proposed metasurface realizes the broadband LP-to-LP and LP-to-CP conversion responses at the same time, as demonstrated by a PCR coefficient that is greater than 90% in the frequency range of 1.39-3.6 THz that realized LP conversion and around 50% in the frequency ranges of 1.08-1.24 THz and 3.65 - 5.27 THz that proved CP conversion, respectively. It is evident that the proposed metasurface can effectively work as a wideband polarization converter.

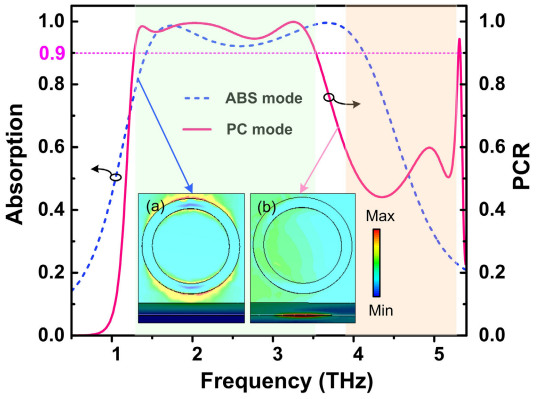

FIGURE 3. Absorption and linear polarization conversion ratio as a function of frequency under normal incidence. The inset shows the electric field distribution of the multi-functional wideband metasurface for (a) absorption mode (VO_2 is in its fully metallic state) and (b) polarization conversion mode (VO_2 is in its insulating state) at 1.7 THz.

To verify the working mechanism of the proposed metasurface, we simulate the electric field distribution at 1.7 THz for both metallic and insulator states of VO_2. As seen in the inset of Fig. 3 (a), when the VO_2 is in its fully metallic state, the distribution of the electric field is mainly focused on the top VO_2 resonator surface. It indicates that the highly efficient and ultra-broadband absorption is attributed to the top MIM configuration due to the blocking EM wave of the continuous VO_2 metallic layer. Once the VO_2 is in its insulator state, the distribution of the electric field is almost concentrated in the middle gold DSER resonator, as illustrated in the inset of Fig. 3 (b), indicating the polarization conversion ability is originated from the bottom MIM configuration. These obtained results evidence that by tailoring the phase of the continuous VO_2 layer from metallic to insulator phase, this layer can transfer its function from preventing to transmitting the EM incidence wave through the proposed metasurface structure, leading to the switch between the perfect ABS and high-efficiency PC. In the next sections, we will further investigate the performance of the ABS and PC modes of the suggested metasurface.

B. ABSORPTION ANALYSIS

To investigate the absorption performance of the proposed metasurface when working as an absorber, we simulate the dependence of absorption spectra on the incident angle (θ) and polarization angle (φ) for both TE and TM modes, as depicted in Fig. 4. The designed structure exhibits different absorption performance for TE and TM modes with increasing the incidence angle, as seen in Fig. 4. It was reported that the metamaterial perfect absorbers show different absorption properties for TE and TM mode waves due to the shape of resonators [53]. However, the designed metasurface structure keeps the absorptivity above 80% in the ultra-wideband in the range of 1.42 - 4.13 THz with the

wide incidence angle up to 50° for TE mode (Figs. 4(a,b)) and 60° for TM mode (Figs. 4(d,e)). Meanwhile, the absorption spectra are not varied by the change in polarization angles for both TE and TM modes, as shown in Figs. 4(c,f)), respectively. The obtained polarization insensitivity of this structure is due to its symmetry structure of the top metallic VO_2 resonator. These obtained results indicate that the proposed metasurface can operate as an absorber device with high-efficiency, ultra-wideband as well as wide-angle incidence and polarization insensitivity.

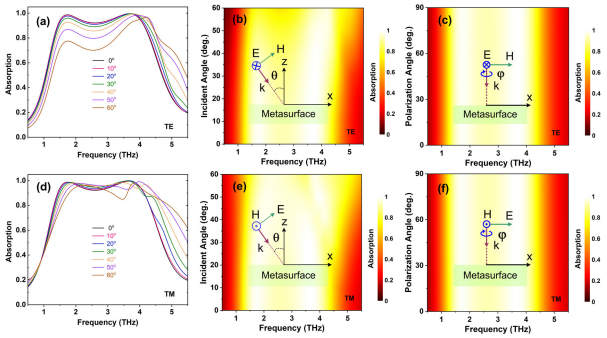

FIGURE 4. The absorption performance at various incidence angles for (a,b) TE and (d,e) TM modes represented by selected lines and color contour, respectively and polarization angles for (c) TE and (f) TM modes when VO_2 is in its fully metallic state.

Fig. 5 shows the good impedance matching between the metasurface and air in the broadband from 1.42 THz to 4.13 THz. This observation explains the achieved wideband absorption spectrum of the metasurface when VO_2 stays in its metallic phase. It is evidenced by the real part and the imaginary components of the normalized impedance of approximately 1 and 0, respectively, as illustrated in Fig. 5, which are determined by using Eq. 8 [46], [54]:

$$Z(\omega) = \sqrt{\frac{(1+S_{11}(\omega))^2 - S_{21}(\omega)^2}{(1-S_{11}(\omega)^2 - S_{21}^2(\omega)}} = \frac{1+S_{11}(\omega)}{1-S_{11}(\omega)} \quad (8)$$

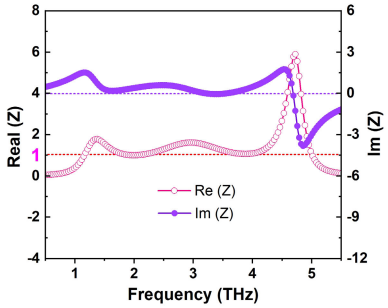

FIGURE 5. The normalized input impedance of a unit-cell of the multi-functional metasurface as a function of frequency under normal incidence when VO_2 is in its fully metallic state.

To study the physics behind the operation mechanism, an equivalent circuit model of a unit cell of the proposed multi-functional metasurface is established using transmission line theory [55], as illustrated in Fig. 6(a). Due to the

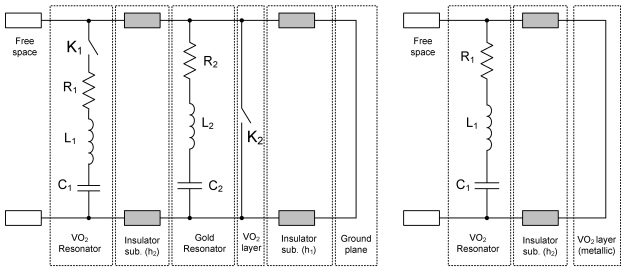

FIGURE 6. (a) The equivalent circuit of a unit-cell of the entire multi-functional metasurface structure and (b) its corresponding equivalent circuit for absorption mode (VO_2 is in its fully metallic state).

phase change of VO_2 materials, switches (K_1 and K_2) are used to distinguish the phase change of VO_2 from metallic state to insulation state. The switches (K_1 and K_2) stay at ON state when VO_2 is in its fully metallic state and at OFF state when VO_2 is in its insulating state. The equivalent circuit model consists of a transmission line of free space, an $R_1L_1C_1$ circuit for the metallic VO_2 resonator layer connected with a switch (K_1), a transmission line for the SiO_2 substrate (h_2), an $R_2L_2C_2$ circuit for the gold resonator layer, a VO_2 layer as a switch (K_2), and a transmission line for the SiO_2 substrate (h_1). When VO_2 is in its fully metallic state (K_1=K_2=ON state), the equivalent circuit model is composed of a transmission line of free space, an $R_1L_1C_1$ circuit for the metallic VO_2 resonator layer, a shorted transmission line for the SiO_2 substrate (h_2), as shown in Fig. 6(b). From Fig. 6(b), the value of $Z(\omega)$ depends on the size and shape of the VO_2 resonant structure and the thickness of the SiO_2 substrate. Therefore, by optimizing the sizes of the VO_2 resonant structure and the thickness of the SiO_2 substrate (h_1), the impedance matching condition can be obtained as can be seen in Fig.5, and the perfect absorption can be achieved, as depicted in Fig.3. Meanwhile, when VO_2 is in its insulating state (K_1=K_2=OFF state), the equivalent circuit model is composed of a transmission line of free space, a transmission line of the SiO_2 substrate (h_2), an $R_2L_2C_2$ circuit for the metallic gold resonator layer, a shorted transmission line for the SiO_2 substrate (h_1). Thus, by optimizing the sizes of the gold resonant structure and the thickness of the SiO_2 substrate (h_1), the wideband and high efficiency cross polarization conversion can be obtained, as shown in Fig.3. The optimizing process is shown in the supplement information.

To further investigate the wideband absorption mechanism, the electric field distributions at different resonance frequencies of 1.7 THz and 3.7 THz in the XOY and XOZ planes under normal incidence are investigated, as depicted in Fig. 7. At a lower frequency of 1.7 THz, the electric field is strongly concentrated around the outer ring, and thus the resonance is generated from the electric dipoles that appear between the neighboring rings. Meanwhile, the electric field distribution is accumulated on both sides of the ring at the higher frequency of 3.7 THz. It implies that the resonant

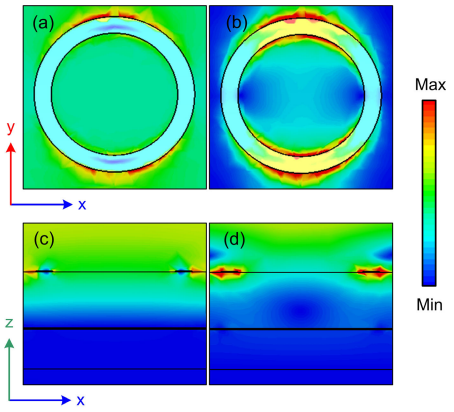

FIGURE 7. The electric field distributions at the resonant frequencies of (a,c) 1.7 THz and (b,d) 3.7 THz in the XOY and XOZ planes when VO_2 is in metallic state, respectively.

frequency of 3.7 THz is associated with two different electric dipole responses. The localized electric field inside the ring is formed by the corresponding electric dipole mode of the inner ring, while the coupled field between the outer rings of neighboring unit cells is owing to the electric dipoles formed by the interaction between the neighboring outer rings. Besides the two sides of the ring supporting different frequency resonances, the high lossy metallic VO_2 compared with other noble metals, resulting in enlarging the absorption band. It was reported that the loss of Cr is lower than that of other noble metals (gold or silver). Therefore, it can reduce the dipole resonances quality factor and enlarge the absorption bandwidth [30], [33].

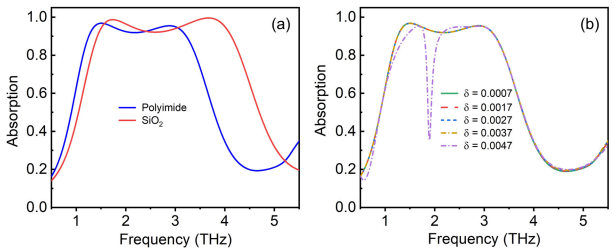

FIGURE 8. The absorption spectra at (a) different substrates and (b) loss tangents of substrate when VO_2 is its fully metallic state.

Furthermore, the effect of different insulator substrates, such as polyimide and various loss tangents of insulator substrates on the absorption spectra of the proposed structure, is investigated when VO_2 is in its fully metallic state, as illustrated in Figs. 8(a) and (b), respectively. The polyimide substrate has a dielectric constant of 3.5 and a loss tangent of 0.0027. The loss tangent of polyimide varies in the range of 0.0007 to 0.0047. As depicted in Fig. 8(a), compared with the proposed structure using SiO_2 substrate, the bandwidth of the proposed structure shrinks in the lower absorption frequency region when polyimide is used as the insulator substrate of the designed structure. However, the proposed structure still exhibited a wideband absorption response with absorptivity above 90%. Thus, the polyimide substrate, which can be fabricated by the low-cost spin coating method, can become a good candidate for the design of a wideband absorber operating in the THz region. Meanwhile, the absorption spectrum of the proposed structure is almost unchanged when the loss tangent is below 0.0027. However, with further increasing the loss tangent, there is a dip at 1.9 THz that occurred in the absorption spectrum, as seen in Fig. 8(b). These observations are caused by the intrinsic properties of substrate materials.

C. POLARIZATION CONVERSION ANALYSIS

Fig. 9(a) shows the magnitude and the phase difference of the reflection coefficients under normal incidence for the y-polarized incidence when VO_2 is in the insulator state. It is clear that the magnitude of cross-reflection coefficients (r_{xy}) is larger than 0.9, while the amplitude of co-reflection coefficients (r_{yy}) is less than 0.2 in the wide frequency range from 1.27 - 3.53 THz, which corresponds to PCR above 90% as seen in Fig. 3. Furthermore, the different phase of the co- and the cross-polarization coefficient $\Delta\phi = \pm 90° + 2k\pi$ in the entire working band. It proves that the designed metasurface can work efficiently as a wideband linear polarization converter. Importantly, the y-polarized incidence wave is reflected with the amplitude of $r_{xy} \simeq r_{yy}$ and phase differences are nearly 90° and 450° at two frequency bands of 1.08-1.24 THz and 3.65 - 5.27 THz, respectively. In addition, the AR is lower than 3 dB and ellipticity reaches to nearly 1 in these frequency ranges (Fig. 9(b)). This means that the reflected wave is the RHCP wave at two frequency bands of 1.08-1.24 THz and 3.65 - 5.27 THz. These observations indicate that this metasurface can transform the LP light into RHCP light at two bands of 1.08-1.24 THz and 3.65 - 5.27 THz simultaneously with cross-polarized light in the wideband of 1.27 - 3.53 THz.

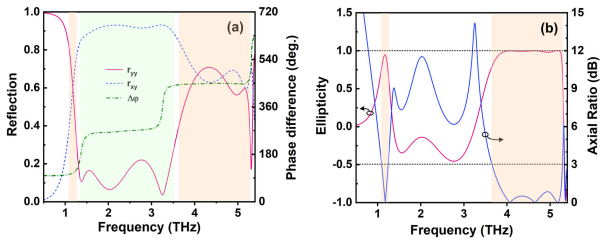

FIGURE 9. (a) Reflection and phase differences and (b) Ellipticity and Axial ratio as a function of frequency under normal incidence when VO_2 is in the insulating state.

To investigate the performance of cross-polarization conversion and circular polarization conversion, we simulate the dependence of the PCR and the ellipticity on the incident angles for both TE and TM modes as shown in Fig. 10 and Fig. 11, respectively. As seen in Fig. 10, when the incident angle increases up to 40°, the PCR value can maintain above 80% in the entire working band from 1.27 - 3.53 THz for both TE and TM modes. In addition, there is a dip that appeared in the working band due to the sharp absorption at this frequency [47], [56]. The obtained result indicates that the designed

structure can work as a cross-polarization converter with a wide incident angle.

Meanwhile, both RHCP bandwidths tend to shrink with increasing incidence angles for both modes, which is due to the destructive interference [57] as seen in Fig. 11. However, the ellipticity value can keep above 80% with incidence angle up to 45° for lower RHCP band and 20° for lower RHCP in both TE and TM modes. These observations demonstrate the stability of the metasurface structure when it works as a polarization converter for both LPC and CPC modes.

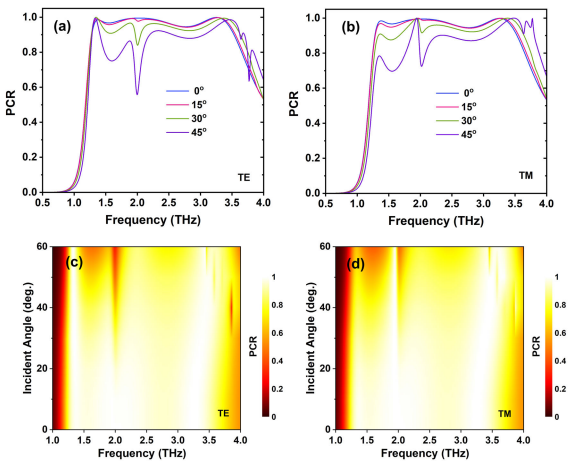

FIGURE 10. Linear-to-linear cross-polarization conversion. PCR at various incidence angles for (a,c) TE and (b,d) TM modes represented by respectively selected lines and color contour when VO_2 is in its insulating state.

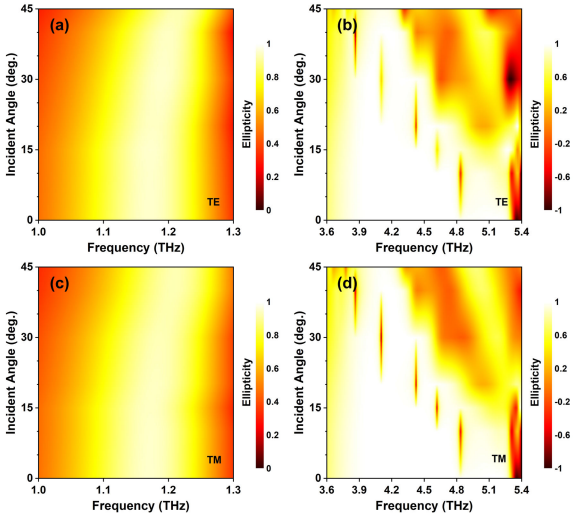

FIGURE 11. Linear-to-circular-polarization conversion. Ellipticity at various incidence angles for (a,b) TE and (c,d) TM modes represented the first and second regions when VO_2 is in its insulating state.

To analyze the physical mechanism of both LPC and CPC of the proposed metasurface, the field decomposition and electric and current distribution are investigated, as shown in Fig. 12. As seen in Fig. 12(a), the incident EM with y-polarization and the reflected wave can decompose into the perpendicular directions of u- and v-directions. The u- and v-axis are rotated ±45° to y-axis, as illustrated in Fig. 12(a). The incident and reflection waves can be decomposed in the uv-coordinate system, as written by Eqs. 9 and 10, respectively [18].

$$E_i = \hat{y}E_i = \hat{u}E_{iu} + \hat{v}E_{iv} \tag{9}$$

$$E_r = \hat{u}E_{ru} + \hat{v}E_{rv} = \hat{u}(r_{uu}E_{iu}e^{i\Phi_{uu}} + r_{uv}E_{iv}e^{i\Phi_{uv}}) + \hat{v}(r_{vv}E_{iv}e^{i\Phi_{vv}} + r_{vu}E_{iu}e^{i\Phi_{vu}}) \tag{10}$$

where $\hat{u}$ and $\hat{v}$ are the unit vectors, r_{uu} and r_{uv}, r_{vv} and r_{vu} and Φ_{uu} and Φ_{uv}, Φ_{vv} and Φ_{vu} are magnitude and phase of co- and cross-reflection coefficients in the u- and v-axis, respectively. If $r_{uu} = r_{vv} \approx 1$, $r_{uv} = r_{vu} \approx 0$, and $\Delta\Phi = |\Phi_{uu} - \Phi_{vv}| = 180° + 2k\pi$ (k is an integer), the synthetic fields of E_{ru} and E_{rv} will be along the x-axis [18]. It suggests that the incoming wave is rotated by 90° and reveals the CPC conversion. On the contrary, if $\Delta\Phi = |\Phi_{uu} - \Phi_{vv}| = 90° + 2k\pi$ (k is an integer), the structure achieves the LP-to-CP conversion. It can be seen in Fig. 12(b), the magnitude of reflections $r_{uu} = r_{vv} \approx 1$ and $r_{uv} = r_{vu} \approx 0$ and the phase difference $\Delta\Phi = 180°$ in the range of 1.08-1.24 THz and $\Delta\Phi = 90°$ in the range of 1.08-1.24 THz and 3.65 - 5.27 THz. These obtained results prove that the proposed structure realizes both LPC in the range of 1.27 - 3.53 THz and CPC in the range of 1.08-1.24 THz and 3.65 - 5.27 THz.

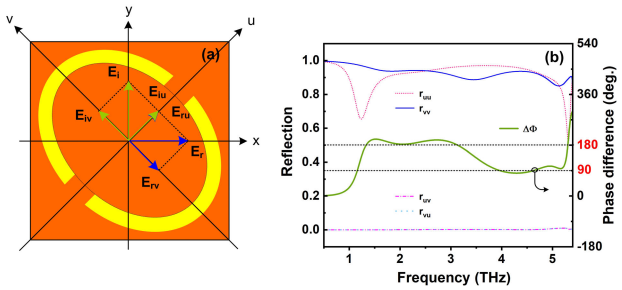

FIGURE 12. (a) The decomposition of the incident and reflection fields in the u- and v-axis. (b) The magnitude of reflections and their phase difference along the u- and v-axis when VO_2 is in its insulating state.

Fig. 13 shows the distributions of electric field and surface current on the top and bottom layers of the gold resonator at different resonant frequencies of 1.37 THz, 2.05 THz, and 3.25 THz. As seen in Figs. 13(a-c), the electric fields are mainly concentrated on the outer edge in the gap of metallic resonator. The resonant frequencies at 1.37 THz, 2.05 THz, and 3.25 THz are caused by the outer edge of the top right and bottom left parts, outer edge of top left and bottom right parts, and the outer edge of both sides of top and bottom parts in the gap, respectively. It was reported the electric and/or magnetic resonances were used to explain the physical mechanism of polarization conversion [18], [47], [57]. When the top and bottom surface currents are parallel, it is known as electric resonance. Conversely, these surface currents are

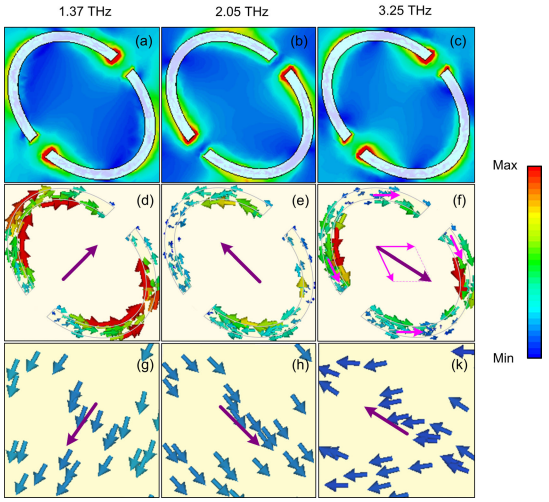

FIGURE 13. The distribution of (a,b,c) electric fields and (d,e,f) the top surface currents, and (g,h,k) the bottom surface currents at various resonant frequencies, respectively when VO_2 is in its insulating state.

TABLE 1. Comparison with the existing state-of-the-art multi-functional metasurfaces in THz range.

Ref.	Function	Operating band (THz)	Efficiency (%)	RBW (%)	Active materials
[38]	ABS	1.54–4.54	ABS>80	96	Graphene
	LPC	2.11–3.63	PCR>90	53	
[30]	ABS	0.562–1.323	ABS>90	74.7	VO_2
	LPC	0.63–1.12	PCR>95	56	
[44]	ABS	0.74–1.62	ABS>90	75	VO_2
	CPC	1.47–2.27	AR<-3dB	42.7	
[37]	ABS	0.67–0.95	ABS>90	34.6	VO_2
	LPC	0.69–1.38	PCR>90	66.7	
[43]	ABS	0.52–1.2	ABS>90	79	VO_2
	LPC	0.42–1.04	PCR>90	85	
[52]	ABS	0.75–1.73	ABS>90	79	Si
	LPC	0.96–1.47	PCR>90	42	
[39]	ABS	1.74–3.52	ABS>90	67	Graphene
	LPC	1.54–2.55	PCR>90	49.3	
	CPC	1.54–2.55	AR<-3dB	49.3	
[32]	ABS	2.17–4.94	ABS>90	77.8	VO_2
	LPC	3.75–4.85	PCR>90	25.8	
	CPC	1.14–1.33&1.78–3.34 &3.566–3.663	AR<-3dB	15.8&60.84 &2.67	
This work	ABS	1.42–4.13	ABS>90	97.7	VO_2
	LPC	1.27–3.53	PCR>90	94.2	
	CPC	1.08–1.24&3.65–5.27	AR<-3dB	13.8&36.3	

anti-parallel, it is known as magnetic resonance. Figs. 13(d-k) show that the surface current of the top layer is anti-parallel with the surface current of the bottom layer for three different resonant frequencies. It reveals that the resonant frequencies are owing to magnetic resonance.

Finally, the performance of our proposed metasurface is compared with recently reported switchable multi-functional metasurfaces in the THz region. Tab. 1 shows the multi-functional metasurface features in terms of functionality, operating band, efficiency, RBW, and active materials for switchable functionality ability. As seen in Tab. 1, the proposed structure has excellent performance, characterized by multiple functionalities and wide RBW, simultaneously. As compared to the switchable multi-functional metasurfaces in [32] and [39], the proposed metasurface realizes a smaller RBW in the CPC function but a higher RBW in both ABS and LPC functions. This comparison emphasizes the novelties and contributions of the proposed design.

IV. CONCLUSION

We numerically proposed a switchable wideband metasurface based on the VO_2 configuration, which realized multiple functions with perfect absorption and two different polarization conversions. When VO_2 is in the metallic phase, the absorption effect can be achieved with an absorptivity above 0.9 in the wide range of 1.42-4.13 THz for a wide incidence angle. The operation mechanism of the wideband absorption response can be attributed to the excitation of electric dipoles and high lossy feature of VO_2 metallic. Once VO_2 serves in the insulator phase, the proposed metasurface is not only proved a linear polarization conversion but also displayed linear-to-linear and linear-to-circular polarization conversions. Specifically, the designed device operated as a cross-polarization converter with a LPC ratio above 0.9 in the frequency range of 1.27-3.53 THz for a wide angle of incidence. In addition, it converted the LP light into RHCP lights with high efficiencies in the frequency ranges of 1.08-1.24 THz and 3.65 - 5.27 THz, respectively. Our proposed structure can open a new approach in designing multi-functional wideband metasurface devices in the terahertz range.

REFERENCES

[1] X. Zang, B. Yao, L. Chen, J. Xie, X. Guo, A. V. Balakin, A. P. Shkurinov, and S. Zhuang, "Metasurfaces for manipulating terahertz waves," *Light, Adv. Manuf.*, vol. 2, no. 2, p. 148, 2021.

[2] V. P. Wallace, E. MacPherson, J. A. Zeitler, and C. Reid, "Three-dimensional imaging of optically opaque materials using nonionizing terahertz radiation," *J. Opt. Soc. Amer. A, Opt. Image Sci.*, vol. 25, no. 12, p. 3120, Dec. 2008.

[3] R. Zhu, T. Qiu, J. Wang, S. Sui, C. Hao, T. Liu, Y. Li, M. Feng, A. Zhang, C.-W. Qiu, and S. Qu, "Phase-to-pattern inverse design paradigm for fast realization of functional metasurfaces via transfer learning," *Nature Commun.*, vol. 12, no. 1, p. 2974, May 2021.

[4] R. Zhu, J. Wang, T. Qiu, Y. Han, X. Fu, Y. Shi, X. Liu, T. Liu, Z. Zhang, Z. Chu, C.-W. Qiu, and S. Qu, "Remotely mind-controlled metasurface via brainwaves," *eLight*, vol. 2, no. 1, pp. 1–11, Jun. 2022.

[5] J. Engelberg and U. Levy, "The advantages of metalenses over diffractive lenses," *Nature Commun.*, vol. 11, no. 1, p. 1991, Apr. 2020.

[6] M. Y. Shalaginov, S. An, Y. Zhang, F. Yang, P. Su, V. Liberman, J. B. Chou, C. M. Roberts, M. Kang, C. Rios, Q. Du, C. Fowler, A. Agarwal, K. A. Richardson, C. Rivero-Baleine, H. Zhang, J. Hu, and T. Gu, "Reconfigurable all-dielectric metalens with diffraction-limited performance," *Nature Commun.*, vol. 12, no. 1, p. 1225, Feb. 2021.

[7] G. Zheng, H. Mühlenbernd, M. Kenney, G. Li, T. Zentgraf, and S. Zhang, "Metasurface holograms reaching 80% efficiency," *Nature Nanotechnol.*, vol. 10, no. 4, pp. 308–312, Apr. 2015.

[8] S. C. Malek, H.-S. Ee, and R. Agarwal, "Strain multiplexed metasurface holograms on a stretchable substrate," *Nano Lett.*, vol. 17, no. 6, pp. 3641–3645, Jun. 2017.

[9] N. Yu, P. Genevet, M. A. Kats, F. Aieta, J.-P. Tetienne, F. Capasso, and Z. Gaburro, "Light propagation with phase discontinuities: Generalized laws of reflection and refraction," *Science*, vol. 334, no. 6054, pp. 333–337, Oct. 2011.

[10] Y. Ran, J. Liang, T. Cai, and H. Li, "High-performance broadband vortex beam generator using reflective Pancharatnam–Berry metasurface," *Opt. Commun.*, vol. 427, pp. 101–106, Nov. 2018.

[11] L. Maiolo, A. Ferraro, F. Maita, R. Beccherelli, E. E. Kriezis, T. V. Yioultsis, and D. C. Zografopoulos, "Quarter-wave plate metasurfaces on electromagnetically thin polyimide substrates," *Appl. Phys. Lett.*, vol. 115, no. 24, Dec. 2019, Art. no. 241602.

[12] Y. Deng, C. Wu, C. Meng, S. I. Bozhevolnyi, and F. Ding, "Functional metasurface quarter-wave plates for simultaneous polarization conversion and beam steering," *ACS Nano*, vol. 15, no. 11, pp. 18532–18540, Nov. 2021.

[13] A. Cala' Lesina, D. Goodwill, E. Bernier, L. Ramunno, and P. Berini, "On the performance of optical phased array technology for beam steering: Effect of pixel limitations," *Opt. Exp.*, vol. 28, no. 21, p. 31637, Oct. 2020.

[14] P. Berini, "Optical beam steering using tunable metasurfaces," *ACS Photon.*, vol. 9, no. 7, pp. 2204–2218, Jul. 2022.

[15] B. Zhang and K.-D. Xu, "Dynamically switchable terahertz absorber based on a hybrid metamaterial with vanadium dioxide and graphene," *J. Opt. Soc. Amer. B, Opt. Phys.*, vol. 38, no. 11, p. 3425, Nov. 2021.

[16] Y. Liu, R. Huang, and Z. Ouyang, "Terahertz absorber with dynamically switchable dual-broadband based on a hybrid metamaterial with vanadium dioxide and graphene," *Opt. Exp.*, vol. 29, no. 13, p. 20839, Jun. 2021.

[17] T. Wang, Y. Zhang, H. Zhang, and M. Cao, "Dual-controlled switchable broadband terahertz absorber based on a graphene-vanadium dioxide metamaterial," *Opt. Mater. Exp.*, vol. 10, no. 2, p. 369, Feb. 2020.

[18] T. N. Cao, M. T. Nguyen, N. H. Nguyen, C. L. Truong, and T. Q. H. Nguyen, "Numerical design of a high efficiency and ultra-broadband terahertz cross-polarization converter," *Mater. Res. Exp.*, vol. 8, no. 6, Jun. 2021, Art. no. 065801.

[19] Y. Li, L. Zeng, and H. Zhang, "Technique for improving polarization conversion performance," *J. Opt. Soc. Amer. B, Opt. Phys.*, vol. 39, no. 10, p. 2573, Oct. 2022.

[20] Y.-P. Li, Z. Qiao, K. Xia, L. Zhang, and H.-F. Zhang, "Electromagnetic resonance modification technique for optimization of polarization conversion performance in metastructures," *IEEE Trans. Antennas Propag.*, vol. 71, no. 10, pp. 8097–8110, Oct. 2023.

[21] Q. Zheng, C. Guo, and J. Ding, "Wideband metasurface-based reflective polarization converter for Linear-to-Linear and linear-to-circular polarization conversion," *IEEE Antennas Wireless Propag. Lett.*, vol. 17, pp. 1459–1463, 2018.

[22] T. K. T. Nguyen, T. M. Nguyen, H. Q. Nguyen, T. N. Cao, D. T. Le, X. K. Bui, S. T. Bui, C. L. Truong, D. L. Vu, and T. Q. H. Nguyen, "Simple design of efficient broadband multifunctional polarization converter for X-band applications," *Sci. Rep.*, vol. 11, no. 1, p. 2032, Jan. 2021.

[23] X. Gao, W. L. Yang, H. F. Ma, Q. Cheng, X. H. Yu, and T. J. Cui, "A reconfigurable broadband polarization converter based on an active metasurface," *IEEE Trans. Antennas Propag.*, vol. 66, no. 11, pp. 6086–6095, Nov. 2018.

[24] X. Pei, H. Yin, L. Tan, L. Cao, Z. Li, K. Wang, K. Zhang, and E. Björnson, "RIS-aided wireless communications: Prototyping, adaptive beamforming, and indoor/outdoor field trials," *IEEE Trans. Commun.*, vol. 69, no. 12, pp. 8627–8640, Dec. 2021.

[25] J. Wang, R. Yang, R. Ma, J. Tian, and W. Zhang, "Reconfigurable multifunctional metasurface for broadband polarization conversion and perfect absorption," *IEEE Access*, vol. 8, pp. 105815–105823, 2020.

[26] L. Dai, B. Wang, M. Wang, X. Yang, J. Tan, S. Bi, S. Xu, F. Yang, Z. Chen, M. D. Renzo, C.-B. Chae, and L. Hanzo, "Reconfigurable intelligent surface-based wireless communications: Antenna design, prototyping, and experimental results," *IEEE Access*, vol. 8, pp. 45913–45923, 2020.

[27] D. H. Le and S. Lim, "Four-mode programmable metamaterial using ternary foldable origami," *ACS Appl. Mater. Interface*, vol. 11, no. 31, pp. 28554–28561, Aug. 2019.

[28] Y. Ma and H. Zhang, "Wide-angle energy steering and magnetic information detection-coding of stacked ferrite-based elements in the gradient magnetic domain," *Opt. Laser Technol.*, vol. 156, Dec. 2022, Art. no. 108544.

[29] M. Zhang, J. Zhang, A. Chen, and Z. Song, "Vanadium dioxide-based bifunctional metamaterial for terahertz waves," *IEEE Photon. J.*, vol. 12, no. 1, pp. 1–9, Feb. 2020.

[30] F. Ding, S. Zhong, and S. I. Bozhevolnyi, "Vanadium dioxide integrated metasurfaces with switchable functionalities at terahertz frequencies," *Adv. Opt. Mater.*, vol. 6, no. 9, May 2018, Art. no. 1701204.

[31] Z. Ren, L. Cheng, L. Hu, C. Liu, C. Jiang, S. Yang, Z. Ma, C. Zhou, H. Wang, X. Zhu, Y. Sun, and Z. Sheng, "Photoinduced broad-band tunable terahertz absorber based on a VO_2 thin film," *ACS Appl. Mater. Interface*, vol. 12, no. 43, pp. 48811–48819, Sep. 2020.

[32] Y. Qiu, D.-X. Yan, Q.-Y. Feng, X.-J. Li, L. Zhang, G.-H. Qiu, and J.-N. Li, "Vanadium dioxide-assisted switchable multifunctional metamaterial structure," *Opt. Exp.*, vol. 30, no. 15, p. 26544, Jul. 2022.

[33] T. M. Nguyen, D. L. Vu, T. Q. H. Nguyen, and J.-M. Kim, "Reconfigurable broadband metasurfaces with nearly perfect absorption and high efficiency polarization conversion in THz range," *Sci. Rep.*, vol. 12, no. 1, p. 18779, Nov. 2022.

[34] J. Ge, Y. Zhang, H. Dong, and L. Zhang, "Nanolayered VO_2-based switchable terahertz metasurfaces as near-perfect absorbers and antireflection coatings," *ACS Appl. Nano Mater.*, vol. 5, no. 4, pp. 5569–5577, Apr. 2022.

[35] G. Wang, S. Zuo, J. Liu, X. Zhang, M. Li, S. Yang, Y. Jia, and Y. Gao, "Difunctional terahertz metasurface with switchable polarization conversion and absorption by VO2 and photosensitive silicon," *Phys. Chem. Chem. Phys.*, vol. 25, no. 29, pp. 19719–19726, 2023.

[36] Z. Wang, Q. Chen, Y. Ma, T. Guo, C. Shuai, and Y. Fu, "Design of thermal-switchable absorbing metasurface based on vanadium dioxide," *IEEE Antennas Wireless Propag. Lett.*, vol. 21, pp. 2302–2306, 2022.

[37] Y. Li, L. Zeng, H. Zhang, D. Zhang, K. Xia, and L. Zhang, "Multifunctional and tunable metastructure based on VO2 for polarization conversion and absorption," *Opt. Exp.*, vol. 30, no. 19, p. 34586, Sep. 2022.

[38] L. Peng, X. Jiang, and S.-M. Li, "Multi-functional device with switchable functions of absorption and polarization conversion at terahertz range," *Nanosc. Res. Lett.*, vol. 13, no. 1, p. 385, Nov. 2018.

[39] Z. Li, R. Yang, J. Wang, Y. Zhao, J. Tian, and W. Zhang, "Multifunctional metasurface for broadband absorption, linear and circular polarization conversions," *Opt. Mater. Exp.*, vol. 11, no. 10, p. 3507, Oct. 2021.

[40] J. Peng, Y. She, H. Su, C. Ji, C. Huang, and X. Luo, "A multifunctional reconfigurable absorber enabled by graphene and shape memory alloy," *Adv. Opt. Mater.*, vol. 11, no. 5, Mar. 2023, Art. no. 2202125.

[41] J. Huang, J. Li, Y. Yang, J. Li, J. Li, Y. Zhang, and J. Yao, "Active controllable dual broadband terahertz absorber based on hybrid metamaterials with vanadium dioxide," *Opt. Exp.*, vol. 28, no. 5, p. 7018, Mar. 2020.

[42] M. Liu, H. Y. Hwang, H. Tao, A. C. Strikwerda, K. Fan, G. R. Keiser, A. J. Sternbach, K. G. West, S. Kittiwatanakul, J. Lu, S. A. Wolf, F. G. Omenetto, X. Zhang, K. A. Nelson, and R. D. Averitt, "Terahertz-field-induced insulator-to-metal transition in vanadium dioxide metamaterial," *Nature*, vol. 487, no. 7407, pp. 345–348, Jul. 2012.

[43] Z. Song and J. Zhang, "Achieving broadband absorption and polarization conversion with a vanadium dioxide metasurface in the same terahertz frequencies," *Opt. Exp.*, vol. 28, no. 8, p. 12487, Apr. 2020.

[44] D. Yan, M. Meng, J. Li, J. Li, and X. Li, "Vanadium dioxide-assisted broadband absorption and linear-to-circular polarization conversion based on a single metasurface design for the terahertz wave," *Opt. Exp.*, vol. 28, no. 20, p. 29843, Sep. 2020.

[45] S. Barzegar-Parizi, A. Ebrahimi, and K. Ghorbani, "Terahertz wideband modulator devices using phase change material switchable frequency selective surfaces," *Phys. Scripta*, vol. 98, no. 6, May 2023, Art. no. 065531.

[46] D. T. Phan, T. K. T. Nguyen, N. H. Nguyen, D. T. Le, X. K. Bui, D. L. Vu, C. L. Truong, and T. Q. H. Nguyen, "Lightweight, ultra-wideband, and polarization-insensitive metamaterial absorber using a multilayer dielectric structure for C- and X-band applications," *Phys. Status Solidi B*, vol. 258, no. 10, Oct. 2021, Art. no. 2100175.

[47] X. Gao, X. Han, W.-P. Cao, H. O. Li, H. F. Ma, and T. J. Cui, "Ultrawideband and high-efficiency linear polarization converter based on double V-shaped metasurface," *IEEE Trans. Antennas Propag.*, vol. 63, no. 8, pp. 3522–3530, Aug. 2015.

[48] X. Li, S. Tang, F. Ding, S. Zhong, Y. Yang, T. Jiang, and J. Zhou, "Switchable multifunctional terahertz metasurfaces employing vanadium dioxide," *Sci. Rep.*, vol. 9, no. 1, p. 5454, Apr. 2019.

[49] M. M. Qazilbash, M. Brehm, B.-G. Chae, P.-C. Ho, G. O. Andreev, B.-J. Kim, S. J. Yun, A. V. Balatsky, M. B. Maple, F. Keilmann, H.-T. Kim, and D. N. Basov, "Mott transition in vo2 revealed by infrared spectroscopy and nano-imaging," *Science*, vol. 318, no. 5857, pp. 1750–1753, 2007.

[50] Y. S. Kim, "Microheater-integrated single gas sensor array chip fabricated on flexible polyimide substrate," *Sens. Actuators B, Chem.*, vol. 114, no. 1, pp. 410–417, Mar. 2006.

[51] M. I. Khan, Z. Khalid, and F. A. Tahir, "Linear and circular-polarization conversion in X-band using anisotropic metasurface," *Sci. Rep.*, vol. 9, no. 1, p. 4552, Mar. 2019.

[52] S. Liao, J. Sui, and H. Zhang, "Switchable ultra-broadband absorption and polarization conversion metastructure controlled by light," *Opt. Exp.*, vol. 30, no. 19, p. 34172, Sep. 2022.

[53] M. Amiri, F. Tofigh, N. Shariati, J. Lipman, and M. Abolhasan, "Wide-angle metamaterial absorber with highly insensitive absorption for TE and TM modes," *Sci. Rep.*, vol. 10, no. 1, Aug. 2020, Art. no. 13638.
[54] S. Bhattacharyya and K. V. Srivastava, "Triple band polarization-independent ultra-thin metamaterial absorber using electric field-driven LC resonator," *J. Appl. Phys.*, vol. 115, no. 6, Feb. 2014, Art. no. 064508.
[55] D. K. Cheng, *Field and Wave Electromagnetics*. London, U.K.: Pearson, 1989.
[56] T. M. Nguyen, H. L. Phan, D. L. Vu, T. Q. H. Nguyen, and J.-M. Kim, "Ultra-wideband and high-efficiency cross-polarization conversion using a double split ring shaped metasurface for C, X, and Ku-band applications," *AIP Adv.*, vol. 12, no. 11, Nov. 2022, Art. no. 115002.
[57] J. Xu, R. Li, J. Qin, S. Wang, and T. Han, "Ultra-broadband wide-angle linear polarization converter based on H-shaped metasurface," *Opt. Exp.*, vol. 26, no. 16, p. 20913, Aug. 2018.

HUU LAM PHAN was born in Ha Tinh, Vietnam, in 1993. He received the B.S. degree from the School of Electronics and Telecommunications, Vinh University, Nghe An, Vietnam, in 2016, and the Ph.D. degree from the University of Ulsan, South Korea. Currently, he is with Van Lang University. His current research interests include metasurfaces-based polarization converters, absorbers, and metalens.

THI QUYNH HOA NGUYEN received the Ph.D. degree in materials engineering from Chungnam National University, South Korea, in 2009. She is an Associate Professor with Vinh University, Vietnam. Her research interest includes synthesis and application of advanced functional materials into electronic, energy, and RF/microwave devices.

JUNG-MU KIM was born in Jeonju, South Korea, in 1977. He received the B.S. degree in electronic engineering from Ajou University, Suwon, South Korea, in 2000, and the M.S. and Ph.D. degrees in electrical engineering and computer science from Seoul National University, Seoul, South Korea, in 2002 and 2007, respectively. From 2007 to 2008, he was a Postdoctoral Fellow with the University of California, San Diego. In 2008, he joined the Faculty of the Division of Electronic Engineering, Jeonbuk National University, Jeonju, where he is currently a Full Professor. His research interests include the IMU, SPR sensor, RF MEMS for 5G and ink-jet printing, and 3-D printing-based printed electronics.